Semi-Annual Status Report

On

"A Theoretical Investigation of Wing Rocking"

(NASA-CR-165058) A THEORETICAL INVESTIGATION OF WING ROCKING Semiannual Status Report, 1 Jul. - 31 Dec. 1981 (Kansas Univ. Center for Research, Inc.) 36 p HC A03/MF A01 CSCL 01A G3/05

N82-15031

Unclas 08716

NASA Grant NAG 1-134

July 1, 1981 - December 31, 1981

by

C. Edward Lan

and

Chung-Hao Hsu

The Flight Research Laboratory

The University of Kansas Center for Research, Inc.

Lawrence, Kansas 66045

EFFECTS OF VORTEX BREAKDOWN ON LONGITUDINAL AND LATERAL - DIRECTIONAL AERODYNAMICS OF SLENDER WINGS BY THE SUCTION ANALOGY

by

C. Edward Lan and Chung-Hao Hsu

Department of Aerospace Engineering

University of Kansas

Lawrence, Kansas 66045

INTRODUCTION

Theoretical investigation of the breakdown of an isolated vortex has been conducted before (Refs. 1 and 2). However, its application to slender-wing aerodynamics is quite limited in scope and versatility (Ref. 3). In fact, very few correlations with data have been reported. In addition, these available theoretical methods require lengthy computer time and hence, are not suitable for applications in a preliminary design.

In this paper, a semi-empirical method to predict effects of vortex breakdown on aerodynamic characteristics of slender wings is described. The method is based on Polhamus' method of suction analogy. Both longitudinal and lateral-directional characteristics can be predicted.

THEORETICAL DEVELOPMENT

In the method of suction analogy, the vortex lift is equated to the edge suction force in the attached flow. It was observed by Lamar (Ref. 4) that for delta wings the angles of attack for vortex breakdown at the trailing edge (α_{BDTE}) can be related to the leading-edge suction distribution ($C_s C$). For a large α_{BDTE}, the $C_s C$ - distribution tends to peak out at a more outboard location (Fig. 1). However, the location of $(C_s C)_{max}$ itself is not a good correlation parameter because for lower swept wings, such as the 60-deg. delta, th peak location is less distinguished.

Therefore, the method to be developed must (1) employ a good correlation parameter for α_{BDTE} applicable to most planforms, not just delta wings; (2) be able to predict the progression of the breakdown point when $\alpha > \alpha_{BDTE}$; and (3) predict the amount of remaining vortex lift in the region of breakdown. These are described in the following for both longitudinal and lateral-directional aerodynamics.

Longitudinal Aerodynamics

Let

$$\bar{C}_s = \frac{C_s c}{\bar{c} \sin^2 \alpha} \tag{1}$$

where $\bar{c}$ is the mean aerodynamic chord. Since C_s is proportional to $\sin^2\alpha$, it follows that $\bar{C}_s$ is a function of planform and Mach number only. If $\bar{y}_c$ is the nondimensional centroid location of the $\bar{C}_s$ - distribution from inboard to $\bar{y}$ of $\bar{C}_{s(max)}$, it was found that $\bar{y}_c$ correlated well with experimental α_{BDTE} as shown in Fig. 2. The relation between $\bar{y}_c$ and $\bar{y}_\ell$ is illustrated in Fig. 1. The experimental α_{BDTE} are taken from Reference 5. The correlation curve in Fig. 2 was obtained by a least-square analysis of Wentz data (Ref. 5) and can be described as follows,

$$\alpha_{BDTE} = 21.95 - 33.734\,\bar{y}_c + 60.81\,\bar{y}_c^2 - 33.631\,\bar{y}_c^3 + 9.391\,\bar{y}_c^4 - 0.958\,\bar{y}_c^5 \text{ , deg. , if } \bar{y}_c < 2.5 \tag{2a}$$

$$\alpha_{BDTE} \cong 38.0 \text{ deg. , if } \bar{y}_c \geq 2.5 \tag{2b}$$

In Reference 5, the progression rate of the breakdown point on delta wings was also measured. Note that the progression rate

measured in the water tunnel is somewhat different from that in the wind tunnel (Ref. 6). Although the experimental progression rate is slightly different for different delta wings (Fig. 3), for simplicity, a single curve obtained by a least-square analysis of Wentz data is used in the present analysis. The curve can be described by

$$\Delta\bar{\chi} = 0.0470\,\Delta\alpha - 0.0110\,(\Delta\alpha)^2 + 0.0303\,(\Delta\alpha)^3 - 0.0027\,(\Delta\alpha)^4 + 0.0007\,(\Delta\alpha)^5, \quad \text{if } \Delta\alpha < 8.0 \text{ deg.} \tag{3a}$$

$$\Delta\bar{\chi} = 0.5392 + 0.0226\,\Delta\alpha, \quad \text{if } \Delta\alpha \geq 8.0 \text{ deg.} \tag{3b}$$

where $\Delta\alpha = \alpha - \alpha_{BDTE}$, deg. (4)

and $\Delta\bar{\chi}$ is the nondimensional χ - distance (referred to the root chord) from the trailing edge to the breakdown point. The spanwise location of the breakdown point, $\bar{y}_{BD}$, nondimensionalized with half span, can therefore be obtained as

$$\bar{y}_{BD} = 1.0 - \Delta\bar{\chi} \tag{5}$$

Once the vortex - breakdown point is located on the planform, it is necessary to determine the amount of remaining vortex lift after breakdown. It is well known that the vortex strength after breakdown is decreased, but not vanished. In other words, the sectional $C_\ell c$ at any spanwise station $\eta > \bar{y}_{BD}$ must be multiplied by a factor k which is less than 1.0. To determine k , Wentz data for delta wings were analyzed at $\Delta\alpha = 5$ deg. and compared with results by the Quasi-Vortex-Lattice Method (QVLM) (Ref. 7). The factor k is determined by requiring the QVLM results to match Wentz data as closely as possible through a least-square analysis.

The results are

$$k = 0.181 + 0.304\,\bar{y}_\ell \quad , \text{ if } \bar{y}_\ell < 1.49$$
$$k = 0.951 - 0.208\,\bar{y}_\ell + 0.028\,\bar{y}_\ell^2 \quad , \text{ if } 1.49 \le \bar{y}_\ell \le 3.72 \qquad (6)$$
$$k = 0.5 \quad , \text{ if } \bar{y}_\ell > 3.72$$

The results indicate that different planforms (i.e. different $\bar{y}_\ell$) have different vortex characteristics after breakdown.

Lateral-Directional Aerodynamics

It was shown in Refs. 8 and 9 that in a sideslip, the leading-edge vortex on the windward side is pushed inward and downward, thus inducing additional vortex lift; while on the leeward side, it is pushed outward and upward, and thus inducing less vortex lift. Note that the usual vortex lift, as explained through the suction analogy, is produced by the existence of net upwash at the leading edge, thereby inducing vortex separation. This is called the roll-up type of vortex lift in the present analysis. On the other hand, at a given α the sideslip does not change the net upwash at the leading edge. Therefore, to account for the increase in vortex lift on the windward side due to sideslip, a "displacement-type" vortex lift must be introduced. The flow mechanisms and computational methods for sideslip, yawing and rolling motions are described below.

(1) Vortex lift of the displacement type in sideslip

In general, the leading-edge thrust coefficient is given by (Ref. 10)

$$C_t = \frac{\pi}{2}\,\frac{C^2\sqrt{1 - M^2\cos^2\Lambda_\ell}}{\cos\Lambda_\ell} \qquad (7)$$

where Λ_ℓ is the leading-edge sweep angle, and C is the leading-edge

singularity parameter defined as

$$C = \lim_{x \to x_l} \frac{1}{2} \Delta C_p \left(\frac{x - x_l}{c} \right)^{1/2} \tag{8}$$

Now, in sideslip, ΔC_p is given by (Ref. 11)

$$\Delta C_p = 2\Delta\left(\frac{\partial \phi}{\partial x'} \right) = 2\Delta\left(\frac{\partial \phi}{\partial x} \pm \frac{\partial \phi}{\partial y} \sin\beta \right) = 2\gamma_y \pm 2\gamma_x \sin\beta \tag{9}$$

where x' is the x -coordinate in the freestream direction and γ_x , γ_y are the components of vortex density in the x - and y - directions, respectively. The component, γ_y , is responsible for the longitudinal loading. Since the vorticity vector near the leading edge must be parallel to the leading edge, it follows that

$$\gamma_x \propto \gamma_y \tan\Lambda_l \tag{10}$$

near the leading edge. Hence, by substituting Eqs. (9) and (10) into (8), it is obtained that

$$C = C_\alpha (1 \pm \tan\Lambda_l \sin\beta) \tag{11}$$

where

$$C_\alpha = \lim_{x \to x_l} \gamma_y \left(\frac{x - x_l}{c} \right)^{1/2} \tag{12}$$

is the leading edge singularity parameter due to α for the symmetrical loading. Eq. (11) shows that the singularity parameter due to sideslip can also be interpreted as that produced by the interaction between γ_x and the sideslip velocity at the leading edge:

$$C_\beta = \lim_{x \to x_l} \gamma_x \left(\frac{x - x_l}{c} \right)^{1/2} \sin\beta \tag{13}$$

By squaring Eq. (11) and substituting it into Eq. (7), the leading-edge thrust coefficient in sideslip can be obtained:

$$C_{t(\beta)} = \frac{\pi C_{\alpha}^2 \left(\pm 2 \tan \Lambda_{\ell} \sin \beta + \tan^2 \Lambda_{\ell} \sin^2 \beta \right) \sqrt{1 - M^2 \cos^2 \Lambda_{\ell}}}{2 \cos \Lambda_{\ell}} \tag{14}$$

The resulting thrust is in the direction pointing into the sideslip velocity (Fig. 4a). Hence, the corresponding suction coefficient ($C_{s(\beta)}$) is

$$C_{s(\beta)} = \frac{C_{t(\beta)}}{\sin \Lambda_{\ell}} = C_{s(\alpha)} \left(\pm 2 \sin \beta + \tan \Lambda_{\ell} \sin^2 \beta \right) \tag{15}$$

where

$$C_{s(\alpha)} = \frac{\pi C_{\alpha}^2}{2 \cos^2 \Lambda_{\ell}} \sqrt{1 - M^2 \cos^2 \Lambda_{\ell}} \tag{16}$$

is the suction coefficient for the symmetrical loading.

(2) Vortex lift of the displacement type in yawing

As shown in Fig. 4b, the induced sidewash at (x, y) is

$$\beta_r = - \frac{(x - x_{ref})}{b/2} \bar{r} \quad , \quad \bar{r} = \frac{r b}{2 V_{\infty}} \tag{17}$$

This sidewash varies over the planform, and hence gives rise to "variable sideslip" effect. According to Eq. (15), the corresponding suction coefficient ($C_{s(r)}$) is then

$$C_{s(r)} = C_{s(\alpha)} \left(\pm 2 \beta_r + \beta_r^2 \tan \Lambda_{\ell} \right) \tag{18}$$

(3) Regions without potential flow effect

In the method of suction analogy, the vortex lift is added to the potential-flow lift to obtain the total lift. The potential-flow lift is calculated by summing all attached-flow pressure forces

over the planform. This is used for the situation in which a vortex flow of the roll-up type is involved, such as in the symmetrical loading or due to rolling motion. For a vortex flow of the displacement type, a certain region near the edges has to be excluded in calculating the potential-flow component to avoid over-prediction.

According to Reference 12, the magnitude of $c_s c$ gives a good estimate of the location of vortex lift centroid from the leading edge. Hence, $c_{s(\beta)} c$ and $c_{s(\gamma)} c$ are taken to be the streamwise distances measured from the leading edge to the vortex lift centroids for β and γ modes of motion, respectively. In the present method, regions near the leading edge with $\gamma - \gamma_\beta \leq 2.0 (c_s c)$ are assumed not to have the potential-flow effect. However, if the vortex breakdown is predicted to occur, the vortex flow region tends to enlarge, so that the symmetrical ($c_s c$) will be used.

(4) Boundary layer effect on Roll Damping

The rolling motion induces a change in local angle of attack so that the roll-up type vortex lift will be produced. Its calculation is described in Reference 7.

However, it is known that the conventional attached-flow theory tends to over-predict the roll damping by as much as 20% without accounting for the vortex flow (Ref. 13). One possible reason is that the boundary layer near the wing tip is thickened by the centrifugal effect in rolling, so that the effective angle of attack is reduced. For engineering applications, this effect will be accounted for in the following way.

Note that the boundary layer thickness is a function of skin

friction coefficient (C_f). In Reference 14, a formula for the airfoil lift reduction due to boundary layer thickness is given as

$$\frac{\Delta C_l}{C_l} = -k' \sqrt{C_f} \tag{19}$$

where k' was chosen as 2.0. For a wing in steady rolling, it is assumed that Eq. (19) is applicable at the station of mean aerodynamic chord (MAC). According to Reference 15 (page 599), the thickness of a 2-D turbulent boundary layer can be written as

$$\delta_2 = 0.37\, x_t^{4/5} (\nu / V_\infty)^{1/5} \tag{20}$$

where x_t indicates that δ_2 is to be calculated at the trailing edge and ν is the kinematic viscosity. It follows that the slope of boundary layer is given by

$$\frac{d\delta_2}{dx_t} = 0.37 \times \frac{4}{5} x_t^{-1/5} (\nu / V_\infty)^{1/5} \tag{21}$$

According to Ref. 15(page 607), the boundary layer thickness on a rotating disk is given by

$$\delta_3 = 0.526\, \bar{y}^{3/5} (\nu / \omega)^{1/5} \tag{22}$$

where $\bar{y}$ in the present application is taken to be the y - coordinate of MAC and ω is the rotating speed. It follows that

$$\frac{d\delta_3}{d\bar{y}} = 0.526 \times \frac{3}{5} \bar{y}^{-2/5} (\nu / \omega)^{1/5} \tag{23}$$

As shown in Fig. 5, in the present 3 - D applications, $\frac{d\delta_2}{dx_t}$ is taken normal to the trailing edge. The effect of steady rolling is regarded as a small perturbation to the angle-of-attack effect,

so that only its component along the trailing edge will be accounted for. The angle, β_t , for the direction of combined slopes is then given by

$$\tan\beta_t = \frac{\frac{d\zeta_1}{d\bar{y}}\cos\Lambda_t}{\frac{d\zeta_2}{d\bar{x}_t}} = \frac{0.6366\times\frac{2}{\pi}\cos\Lambda_t}{0.39\times\frac{2}{\pi}}\left(\frac{V_\infty \bar{x}_t}{\bar{y}^2\omega}\right)^{1/2} \tag{24}$$

However,

$$\omega\bar{y} = \frac{\omega b}{2V_\infty}\frac{V_\infty}{b/2}\bar{y} = \bar{P}\frac{\bar{y}}{b/2}V_\infty \quad , \quad \bar{P} = \frac{\omega b}{2V_\infty} \tag{25}$$

Hence,

$$\frac{V_\infty \bar{x}_t}{\bar{y}^2\omega} = \frac{V_\infty \bar{x}_t}{\bar{P}\left(\frac{\bar{y}}{b/2}\right)\bar{y}V_\infty} = \frac{b/2}{\bar{y}}\,\frac{\bar{x}_t}{\bar{y}}\,\frac{1}{\bar{P}} \tag{26}$$

Substituting Eq. (26) into Eq. (24), it is obtained that

$$\tan\beta_t = 1.0662\cos\Lambda_t\left(\frac{b/2}{\bar{y}}\,\frac{\bar{x}_t}{\bar{y}}\,\frac{1}{\bar{P}}\right)^{1/2} \tag{27}$$

where

$$\bar{x}_t = \bar{c}\cos\Lambda_t \tag{28}$$

It is assumed that if Eq. (19) is for the angle-of-attack effect, then the combined effect , given by Eq. (19), is increased by a factor of $1/\cos\beta_t$ with β_t given by Eq. (27). With the local angle of attack due to steady rolling, α_p , replacing ζ_y in Eq. (19). Eq. (19) is now rewritten as

$$\frac{\Delta\alpha_p}{\alpha_p} = -2.2\sqrt{c_f}\,\frac{\cos\Lambda_t}{\cos\beta_t} \tag{29}$$

where the constant k' is taken as 2.2, instead of 2.0, for a better

correlation with data, and $\cos\Lambda_t$ is included for the notching effect of the trailing edge. That is, the component, $\frac{d\delta_3}{d\bar{y}}\sin\Lambda_t$, shown in Fig. 5 will make the trailing-edge boundary layer thinner.

(5) Rolling and yawing at non-zero sideslip

It was shown in Reference 8 that the roll damping of a slender wing at high angles of attack can be increased if the wing rolls about the stability axes at a non-zero sideslip. To explain this effect, let the total leading-edge singularity parameter be

$$C = C_\alpha (1 \pm \tan\Lambda_l \sin\beta) + C_\alpha (\pm \beta_r \tan\Lambda_l) + C'_{(p)} + C'_{(\beta)} + C'_{(r)} \tag{30}$$

where $C'_{(p)}$, $C'_{(\beta)}$ and $C'_{(r)}$ are leading-edge singularity parameters produced by upwash (i.e. the roll-up effect), respectively. By squaring C to be used in Eq. (7), various cross-product terms appear. For the rolling motion, the vortex lift due to roll-up is further increased on the right wing due to inboard displacement of vortex core in positive sideslip. Similarly, any roll-up effect in the yawing motion will be further increased or decreased due to sideslip. However, products of any two roll-up effects or displacement effects do not produce forces and moments of the antisymmetrical nature. Hence, additional vortex-lift terms in the leading-edge singularity parameter due to rolling and yawing in sideslip are

$$C^2_{(p\beta)} = 2\, C'_{(p)} (C_\alpha \tan\Lambda_l \sin\beta) \tag{31}$$

$$C^2_{(r\beta)} = 2\, C'_{(r)} (C_\alpha \tan\Lambda_l \sin\beta) \tag{32}$$

Eqs. (31) and (32) are to replace C^2 in Eq. (7) to produce the additional leading-edge thrust.

(6) Vortex breakdown in sideslip

In general, the angle of attack for vortex breakdown at the trailing edge in sideslip, α'_{BDTE}, is reduced on the windward side and increased on the leeward side. The following steps are used to calculate α'_{BDTE} in the present analysis.

(a) Calculate $\bar{\gamma}_\ell$ from the symmetrical suction distribution ($C_{S(\alpha)}$), except that the leading-edge sweep angle is taken to be $\Lambda_\ell - \beta$ for the right wing and $\Lambda_\ell + \beta$ for the left wing.

(b) Assume that the maximum vortex strength before breakdown for a given planform is unchanged by sideslip. Since the vortex strength is represented by C_S which is proportional to $\sin^2\alpha$, it follows that the maximum vortex strength will be reached at a lower α than α_{BDTE} on the right wing because of increase in vortex lift in sideslip. Hence, α'_{BDTE} can be solved from the following equation

$$\sin^2\alpha_{BDTE} = \sin^2\alpha'_{BDTE} + \left(\pm 2\sin\beta + \tan\Lambda_\ell \sin^2\beta\right)\sin^2\alpha'_{BDTE} \quad (33)$$

(c) The vortex lift factor (k_β) is calculated by the same formula for k (i.e. Eq. (6)), except that $\bar{\gamma}_\ell$ is replaced by $\bar{\gamma}_{\ell(\beta)}$ calculated in step (a).

(d) Whenever the vortex breakdown is predicted to occur at a given y station, $C_{S(\alpha)}$ must be multiplied by k. Therefore, the antisymmetrical vortex lift on the windward side due to sideslip would be given by

$$\left(C'_{S(\beta)} + 2\,C_{S(\alpha)}\,k\sin\beta\right)k_\beta$$

On the leeward side, the vortex breakdown may not occur at a given α. In this case, the magnitude of the antisymmetrical vortex lift is the average of those on both sides.

(7) Vortex breakdown in yawing

The effect of yawing on vortex breakdown is similar to that due to sideslip. With a positive yawing, the left tip will be the first which is subject to possible vortex breakdown effect. Since the equivalent sideslip (β_r) is variable along the leading edge, the average of β_r at a given y station and that at the tip is used to determine α'_{BDTE}. For simplicity, α'_{BDTE} for the yawing motion is determined by a linear interpolation between α_{BDTE} and α'_{BDTE} for sideslip.

When the yawing motion occurs at $\beta \neq 0$, the equivalent sideslip to be used should be $-\beta-\beta_r$ on the left wing and $\beta+\beta_r$ on the right wing. Since β_r is usually negative near the tips, the equivalent sideslip there is considerably reduced. In this case, the vortex breakdown may not occur, in particular at a high yaw rate, so that the rolling moment due to yaw rate may be large.

(8) Vortex breakdown in rolling

Due to a positive roll, the local angle of attack on the right wing is increased. It would seem that the vortex-breakdown α would be decreased. However, rolling tends to move outboard the centroid of the vortex lift distribution (i.e. increasing $\bar{y}_\ell$), so that the vortex-breakdown α is increased. In the present theory, it is assumed that α'_{BDTE} for the rolling motion is equal to α_{BDTE} for the symmetrical loading.

The average of the local α at a given y station and that at the tip is used to determine whether there is vortex breakdown at that station.

(9) Centroids of vortex lift

Based on the idea developed in Reference 12, $c_s c$ gives the location of vortex lift centroid. Let leading-edge suction coefficients produced by upwash at the leading edge be denoted by $c'_{s(p)}$, $c'_{s(\beta)}$ and $c'_{s(r)}$. The roll-up for the antisymmetrical vortex lift is assumed to take place along a direction perpendicular to the leading edge. Hence, the antisymmetrical vortex lift of the roll-up type is assumed to act at

$$y - |c'_{s(p)} c| \sin \Lambda_\ell$$

for the rolling motion, and at

$$y - |c'_{s(r)} c| \sin \Lambda_\ell$$

for the yawing motion. In sideslip, it is at

$$y - |c'_{s(\beta)} c| \cos \beta$$

This is illustrated in Fig. 6a.

On the other hand, if rolling and yawing motions take place in a non-zero sideslip, the vortex lift centroids will be at

$$y - |c'_{s(p)} c + c'_{s(\beta)} c| \sin \Lambda_\ell$$

$$y - |c'_{s(r)} c + c'_{s(\beta)} c| \sin \Lambda_\ell$$

For rolling and yawing motions, the inboard displacement of vortex lift centroids is further restricted by the position of symmetrical vortex lift centroids (i.e. $R = c_s c$). Therefore, if

$$|c'_{s(p)} c| \sin \Lambda_\ell > R \cos \Lambda_\ell \sin \Lambda_\ell$$

it is replaced by $R \cos \Lambda_\ell \sin \Lambda_\ell$, where R cannot exceed the local chord. This is illustrated in Fig. 6b.

In a coning motion, rolling and yawing motions are coupled. The vortex lift centroid is then assumed to be that due to the rolling motion.

NUMERICAL RESULTS

Longitudinal Characteristics

Results for delta wings of 60°, 70° and 80° are presented in Figs. 7-10. The method for computing the vortex lift involving rounded leading edges is based on Kulfan's concept (Ref. 16). Note the differences in lift curves after vortex breakdown for different delta wings. The lift curve for the 80-deg. delta has a sharper change after vortex breakdown as compared with that for the 60-deg. delta. The lift curve for the 70-deg. delta wing represents the transition between these two types.

Lateral-Directional Characteristics

The effect of sideslip on the angle of attack for vortex breakdown at the trailing edge is presented in Fig. 11. The trend is correctly predicted, although the predicted magnitude is 2 to 3 deg. off.

The lateral characteristics for 60-deg. and 70-deg. delta wings are presented in Figs. 12 and 13, respectively. The predicted results agree well with data, except when α exceeds α_{BDTE} by 8 to 10 deg. In the latter situation, the effect of boundary layer separation must be accounted for and is not included in the present method.

Additional results are compared with data in Figs. 14, 15 and 16. As shown in Fig. 15, the boundary layer correction is seen to be important for accurate prediction of roll damping. The change in slopes of C_{ℓ_p} and C_{ℓ_ℓ} after vortex breakdown is due to the difference in breakdown α's for left and right wings.

Finally, the effect of sideslip on roll damping is illustrated in Fig. 17. With zero sideslip, the slope of $C_\ell - \bar{p}$ curve is always positive. This means that C_{ℓ_p} is positive. On the other hand, as the sideslip is increased in a steady roll, C_{ℓ_p} may become negative, as shown by the curve

representing $\beta=10^{\circ}$. At $\beta=5^{\circ}$ and small $\bar{p}$, there is some discrepancy between the theory and data.

Extension of the theory to other planform shapes is currently being investigated.

REFERENCES

1. Benjamin, T. B., "Some Developments in the Theory of Vortex Breakdown", Journal of Fluid Mechanics, Vol. 28, 1967, pp. 65-84.

2. Raat, J., "Vortex Development and Breakdown", AIAA Paper 75-881, June 1975.

3. Wilson, J. D., "Calculation of Vortex Breakdown Locations for Flow over Delta Wings", Journal of Aircraft, Vol. 14, Oct. 1977, pp. 1020-1022.

4. Lamar, J. E., "Recent Studies of Subsonic Vortex Lift Including Parameters Affecting Stable Leading-Edge Vortex Flow", Journal of Aircraft, Vol. 14, Dec. 1977, pp. 1205-1211.

5. Wentz, W. H., "Wind Tunnel Investigations of Vortex Breakdown on Slender Sharp-Edged Wings", Ph.D. dissertation, 1968, University of Kansas.

6. Lamar, J. E. and Frink, N. T., "Experimental and Analytical Study of the Longitudinal Aerodynamic Characteristics of Analytically and Empirically Designed Strake-Wing Configurations at Subcritical Speeds", NASA TP-1803, June 1981.

7. Lan, C. E., "Calculation of Lateral-Directional Stability Derivatives of Wings by a Nonplanar Quasi-Vortex-Lattice Method", NASA CR-165659, January 1981.

8. Nguyen, L. T.; Yip, L. and Chambers, J. R., "Self-Induced Wing Rock of Slender Delta Wings", AIAA Paper 81-1883, Aug. 1981.

9. Harvey, J. K., "Some Measurements on a Yawed Slender Delta Wing with Leading-Edge Separation", British ARC, R & M No. 3160, Oct. 1958.

10. Lan, C. E., "A Quasi Vortex-Lattice Method in Thin Wing Theory", Journal of Aircraft, Vol. 11, Sept. 1974, pp. 518-527.

11. Lan, C. E., "Calculation of Lateral-Directional Stability Derivatives for Wing-Body Combinations with and without Jet-Interaction Effects", NASA CR-145251, 1977.

12. Lan, C. E. and Chang, J. F., "Calculation of Vortex Lift Effect for Cambered Wings by the Suction Analogy", NASA CR-3449, July 1981.

13. Lamar, J. E., "Design Charts of Static and Rotary Stability Derivatives for Cropped Double-Delta Wings in Subsonic Compressible Flow", NASA TN D-5661, Feb. 1970.

14. Steinheuer, J., "Boundary Layer Calculation Methods and Application to Aerodynamic Problems", in AGARD-LS-67, "Prediction Methods for Aircraft Aerodynamic Characteristics", 1974.

15. Schlichting, H., "Boundary Layer Theory", 6th Edition, McGraw-Hill, 1968.

16. Kulfan, R. M., "Wing Airfoil Shape Effects on the Development of Leading-Edge Vortices", AIAA Paper 79-1675.

17. Johnson, J. L. Jr., Grafton, S. B. and Yip, L. P., "Exploratory Investigation of the Effects of Vortex Bursting on the High-Angle-of-Attack Lateral-Directional Stability Characteristics of Highly-Swept Wings", AIAA Paper 80-0463.

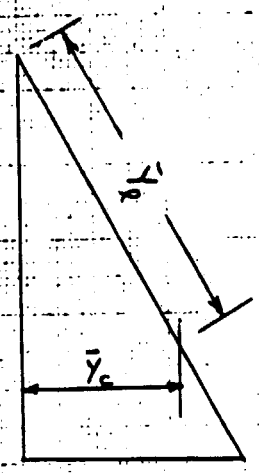

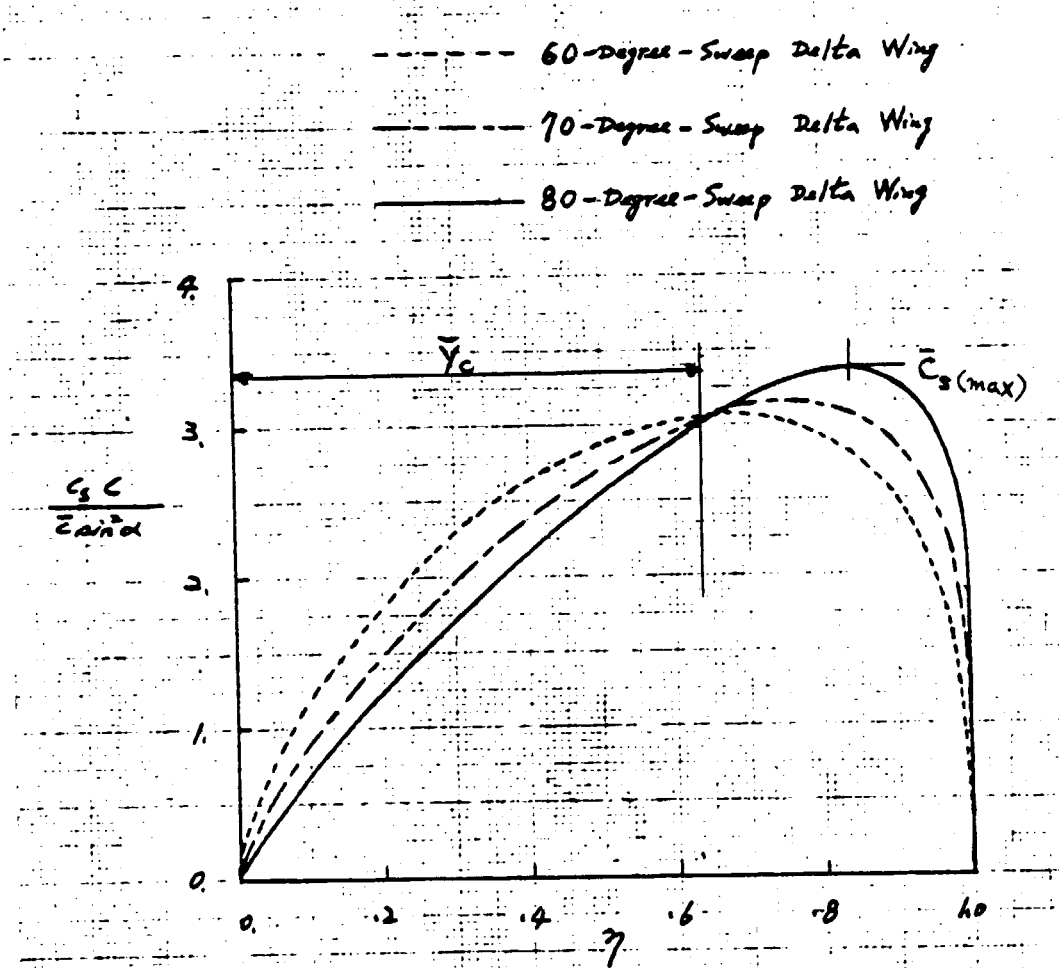

Fig. 1 Leading-Edge Suction Distributions of Delta Wings with Sharp Leading Edges

△ Delta Wing
⏢ Cropped Delta Wing
⏢ Cropped Arrow Wing

Λ_{LE}	75	80	76	70	65	60	55	45	45	45	45	63	63	63
$\frac{c_r}{c_{TE}}$	7.086	3.394	2.266	1.619	1.098	.839	.660	.424	.477	.504	.519	1.141	1.156	1.056
	△	△	△	△	△	△	△	△	⏢ $\lambda=.1$	⏢ $\lambda=.2$	⏢ $\lambda=.3$	⏢ $\lambda=.1$	⏢ $\lambda=.2$	⏢ $\lambda=.29$, $\Lambda_{TE}=38.9°$

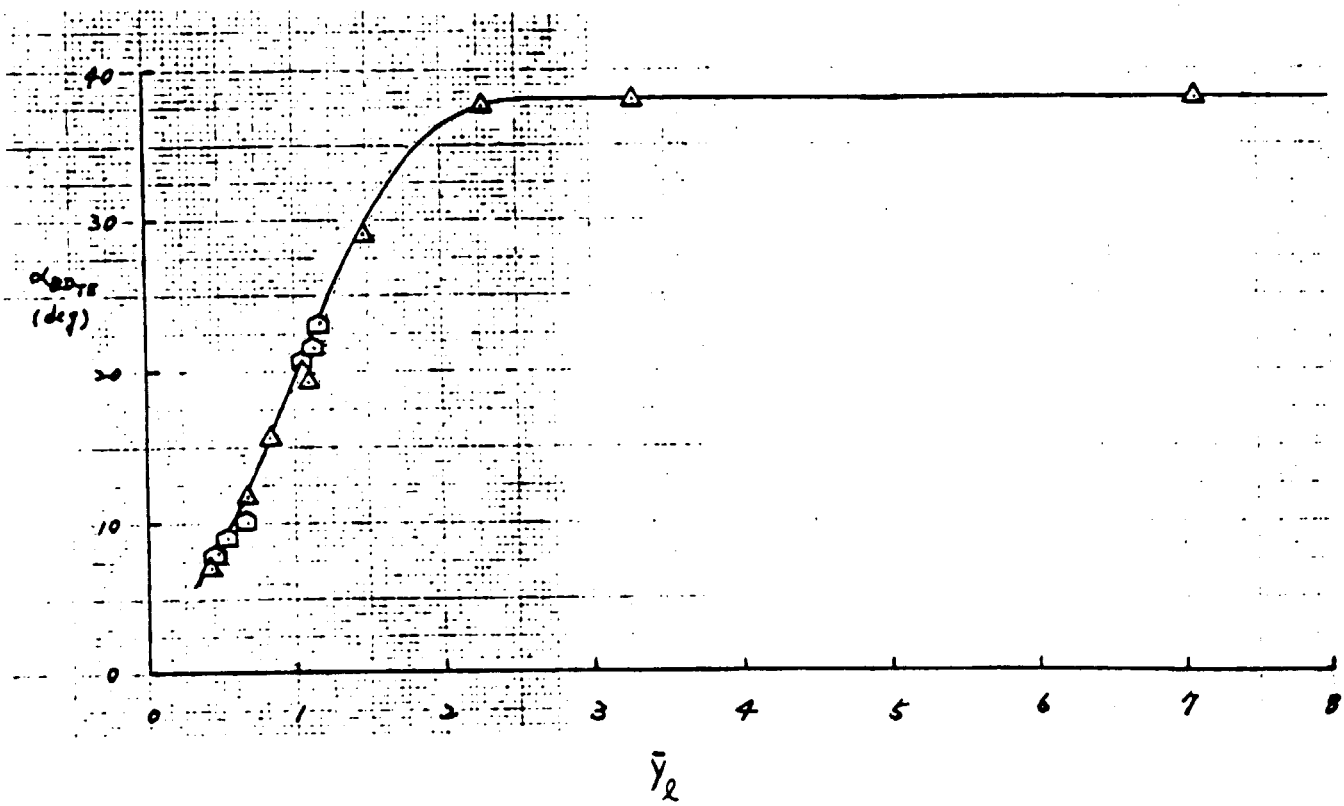

Figure 2. Correlation for Angles of Attack with Vortex Breakdown at the Trailing Edge

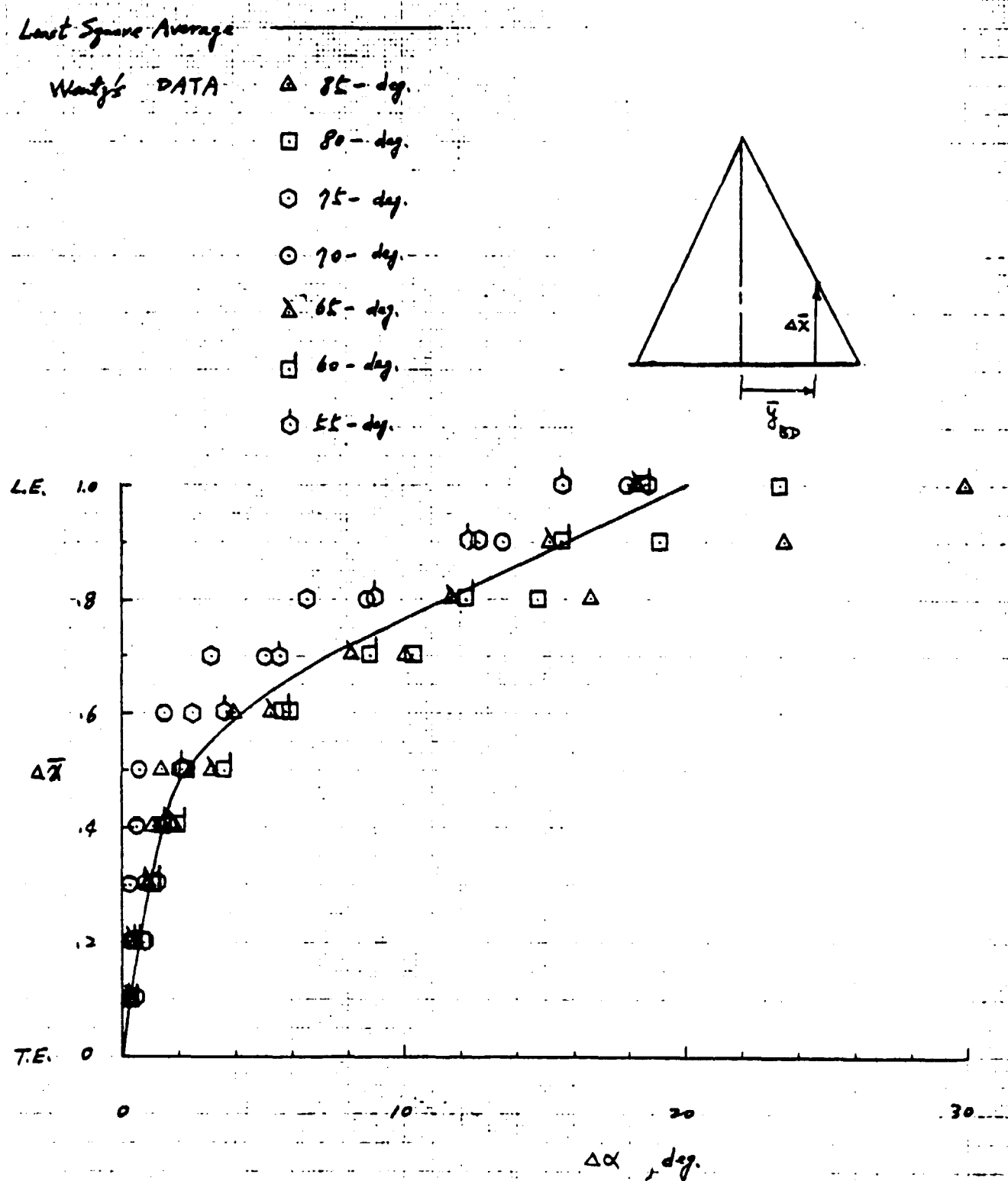

Figure 3. Vortex Breakdown Progression on Delta Wings in Air

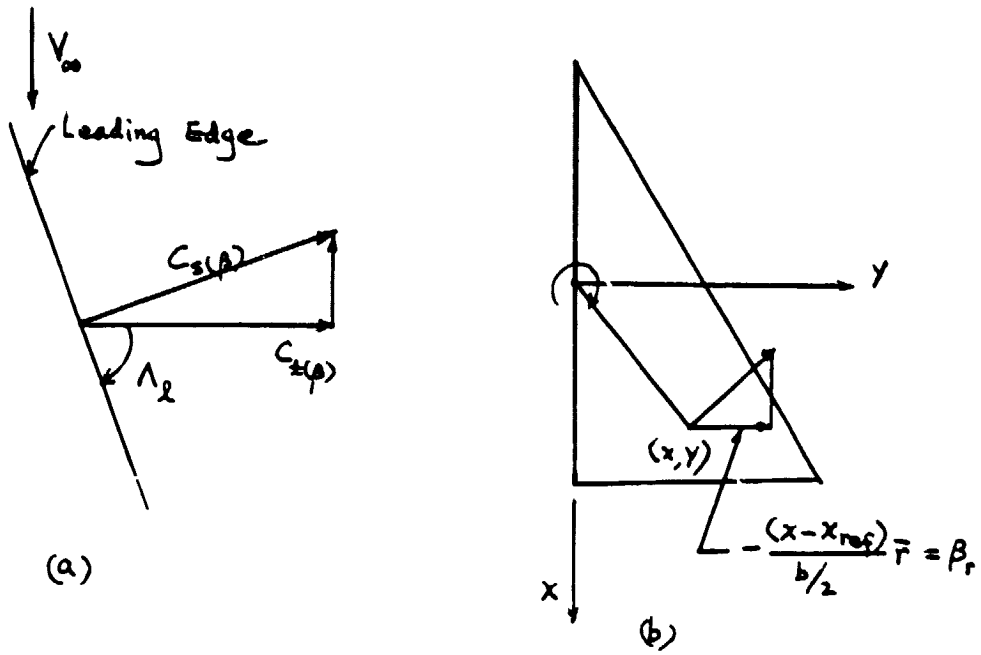

Figure 4 Sideslip Induced Suction and Variable Sideslip due to Yaw

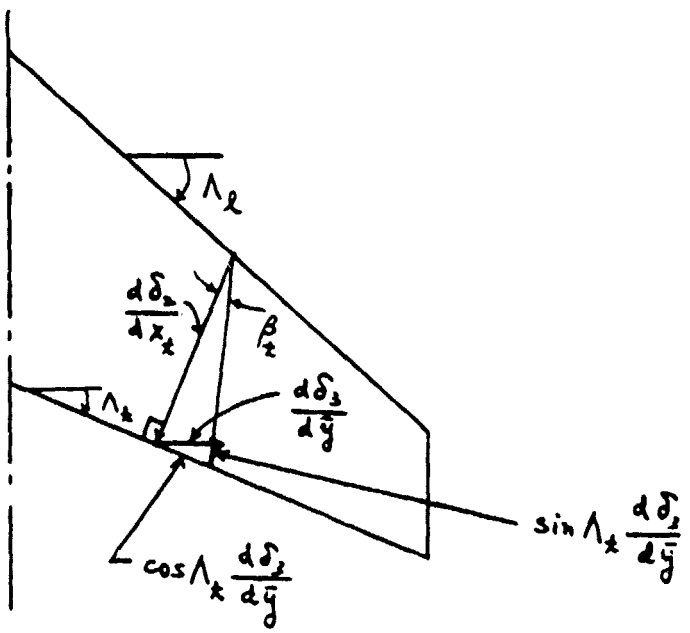

Figure 5 Boundary Layer Surface Slopes due to Angle of Attack and Steady Rolling.

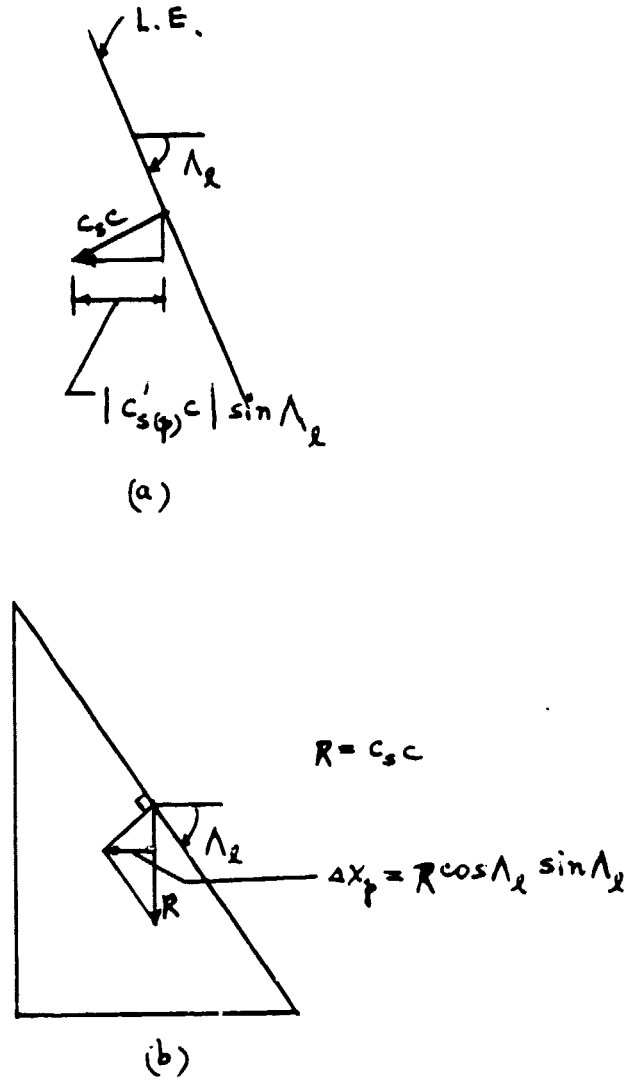

Figure 6. Inboard Displacement of Vortex Lift Centroids in Rolling Motion

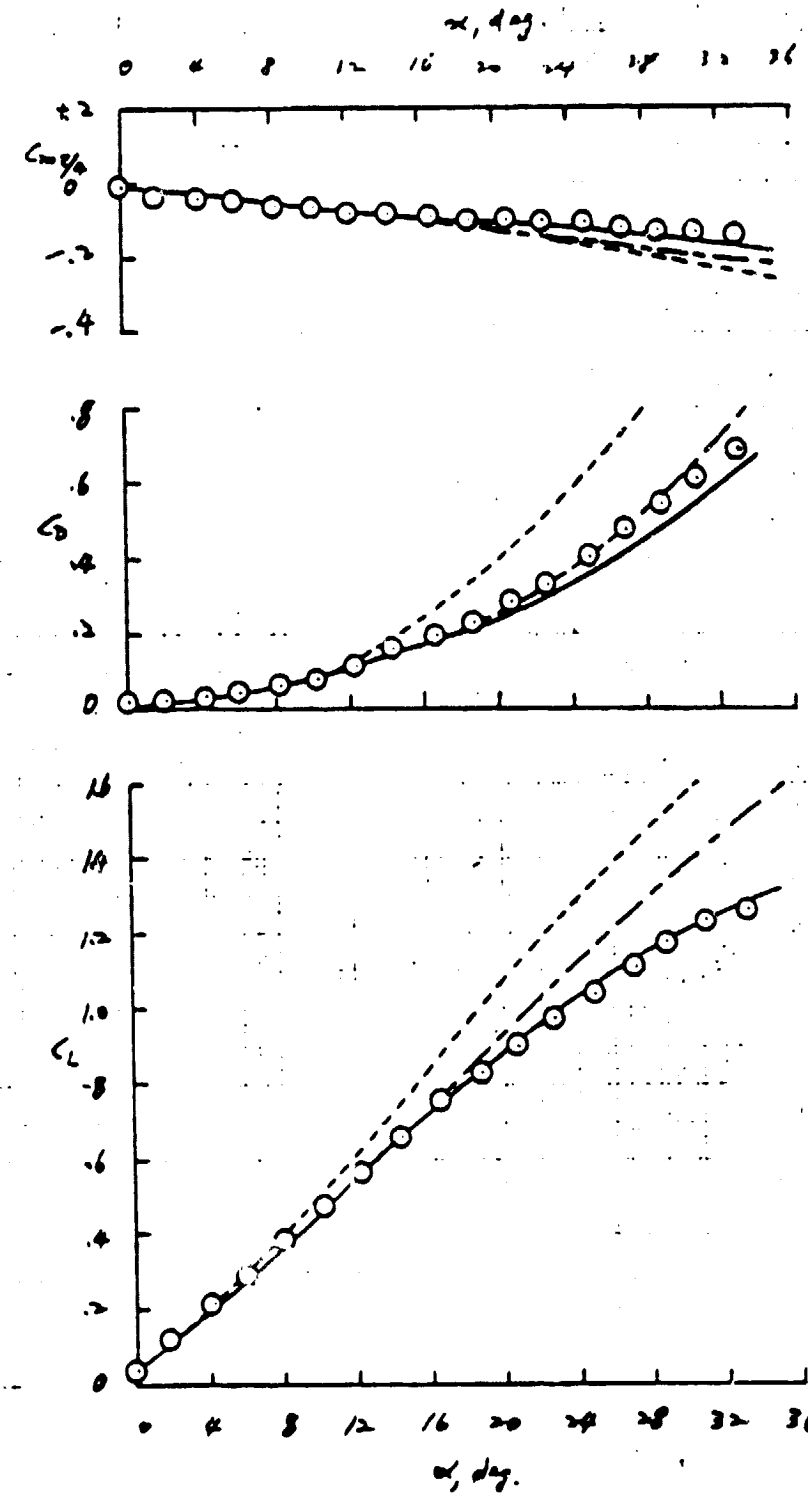

⊙ DATA
(RM L55A07)

Present Theory
——— Rounded L.E. with Vortex Breakdown Effects
– – – – Rounded L.E. without Vortex Breakdown Effects
- - - - Sharp L.E.

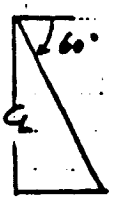

Figure 7 Longitudinal Aerodynamic Characteristics of a Delta Wing of $A = 2.309$ with Rounded Leading Edges

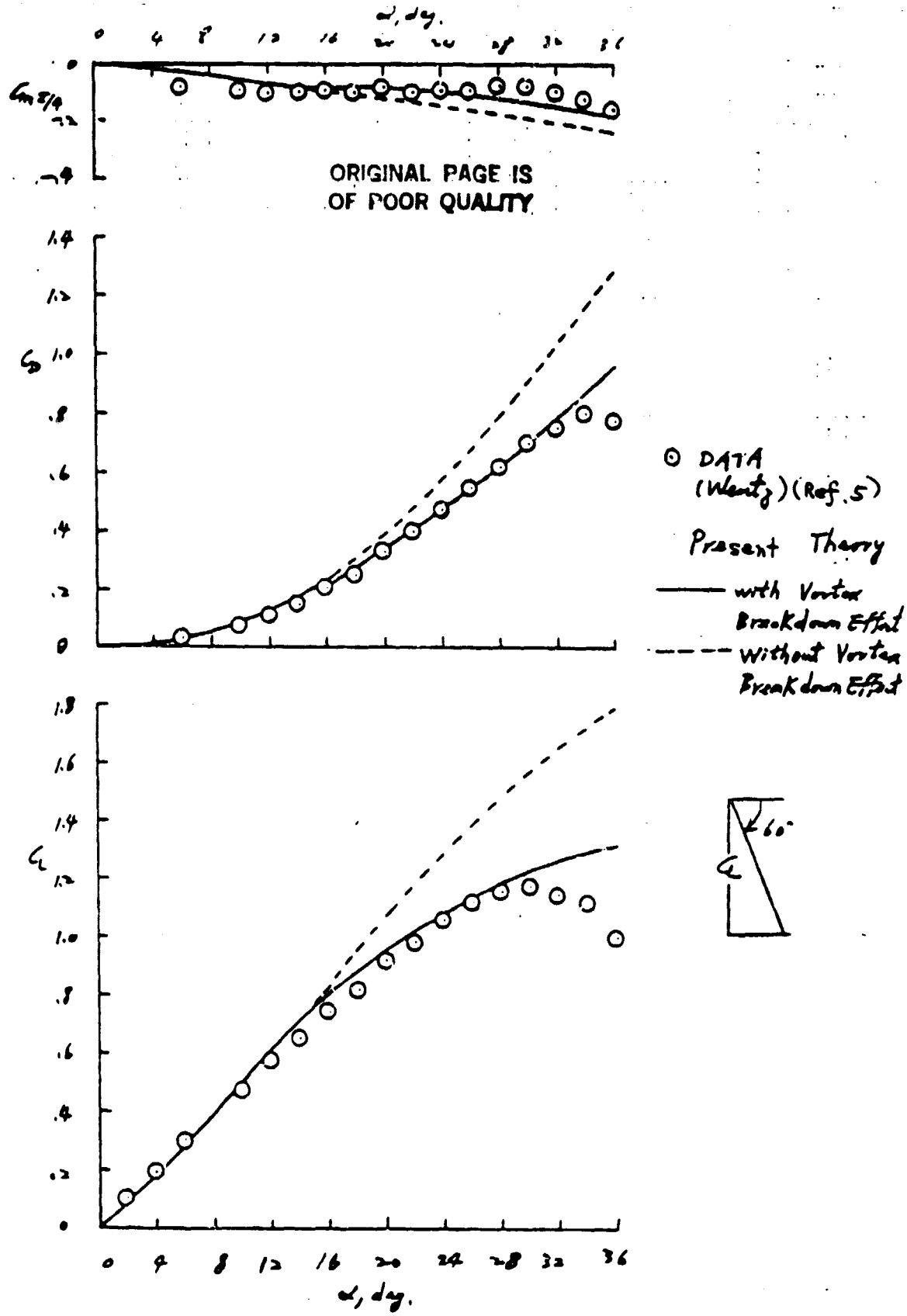

Figure 8 Longitudinal Aerodynamic characteristics of a Delta Wing of $A = 2.309$ with Sharp Leading Edges

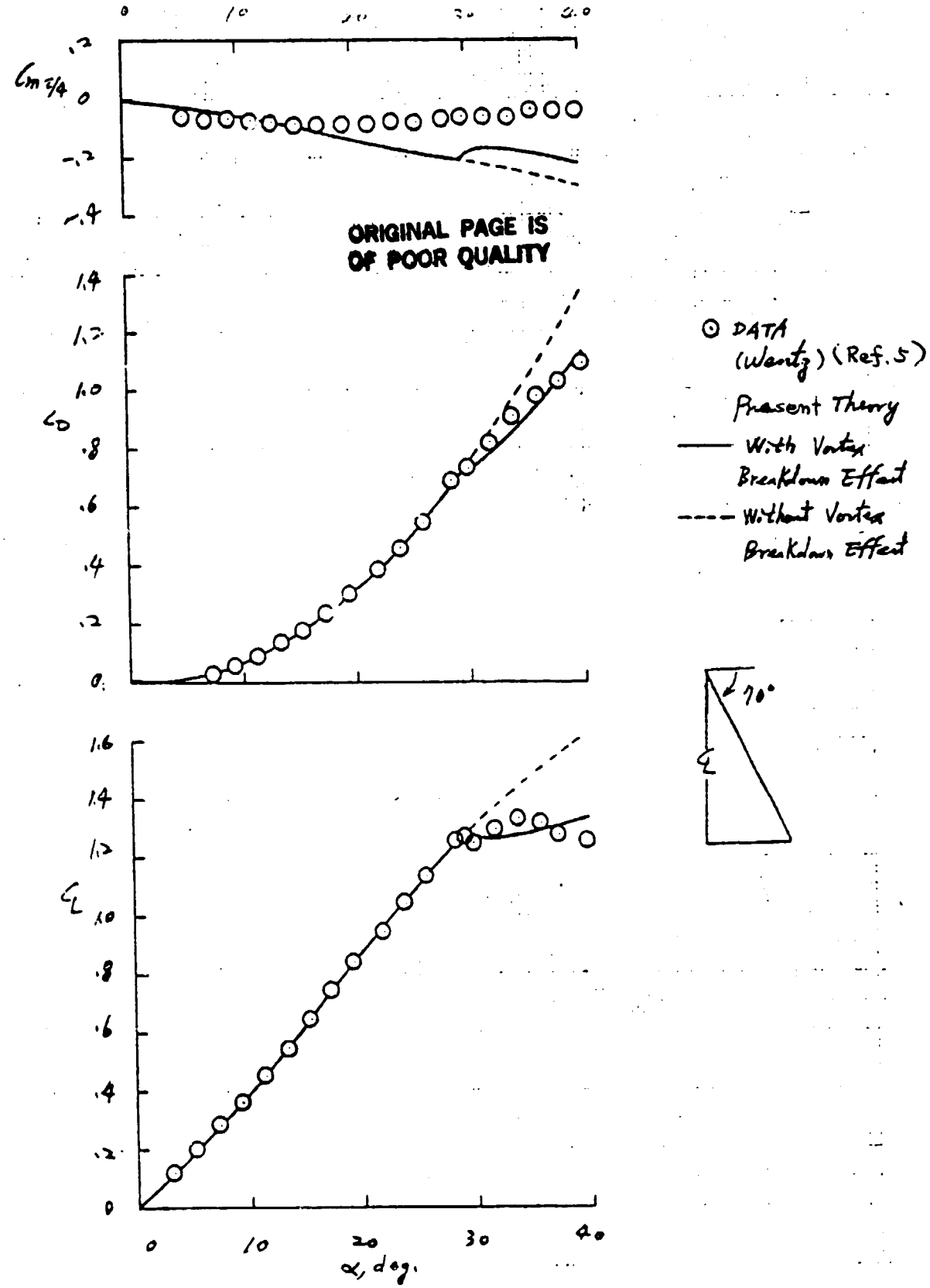

Figure 9 Longitudinal Aerodynamic Characteristics of a Delta Wing of $A = 1.456$ with Sharp Leading Edges

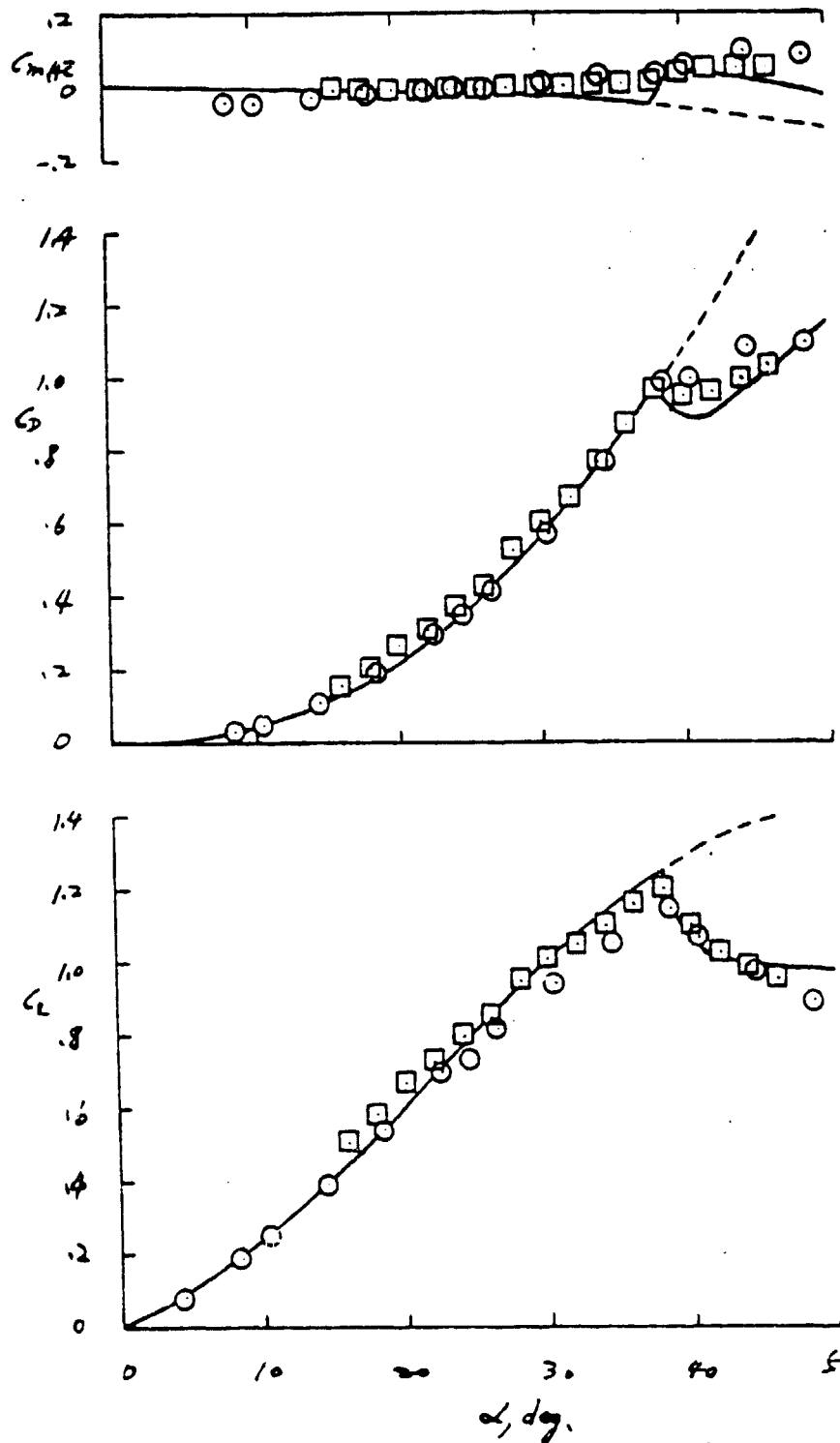

Figure 10 Longitudinal Aerodynamic Characteristics of a Delta Wing of $A = 0.705$ with Sharp Leading Edges

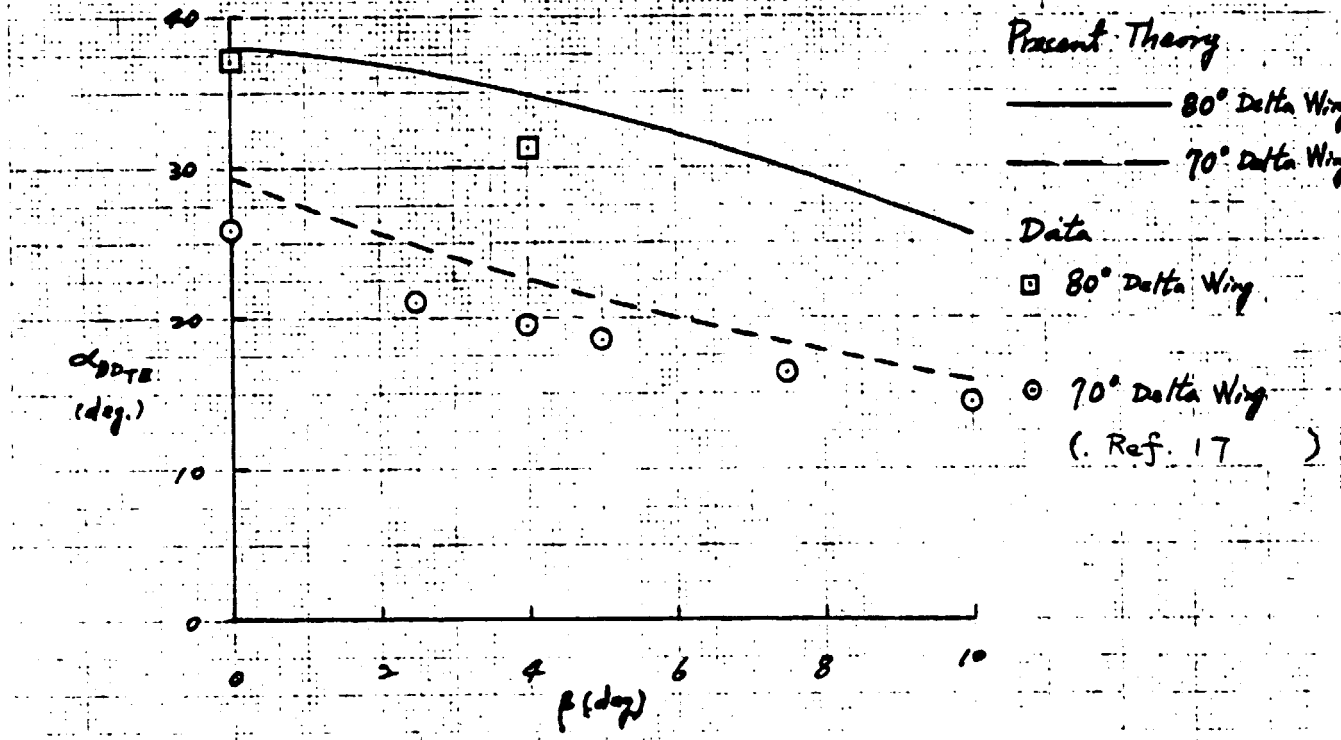

Figure 11 Vortex Breakdown at Trailing Edges of 70° and 80° Delta Wings due to Sideslip

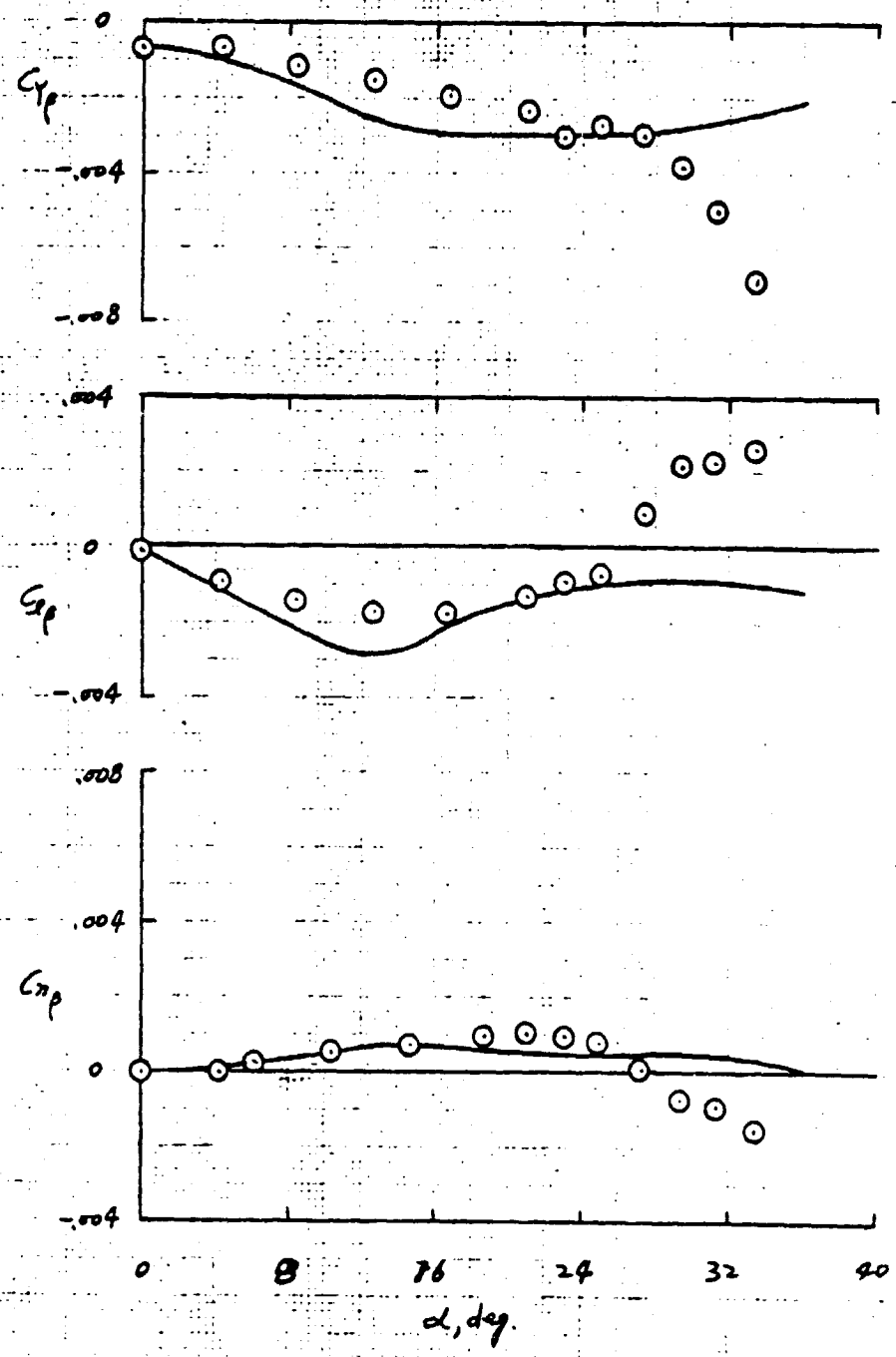

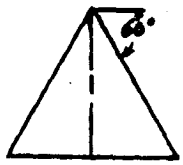

⊙ DATA
(NACA RM L52A07)

Figure 12 Delta Wing of A = 2.309 with Rounded Leading Edges

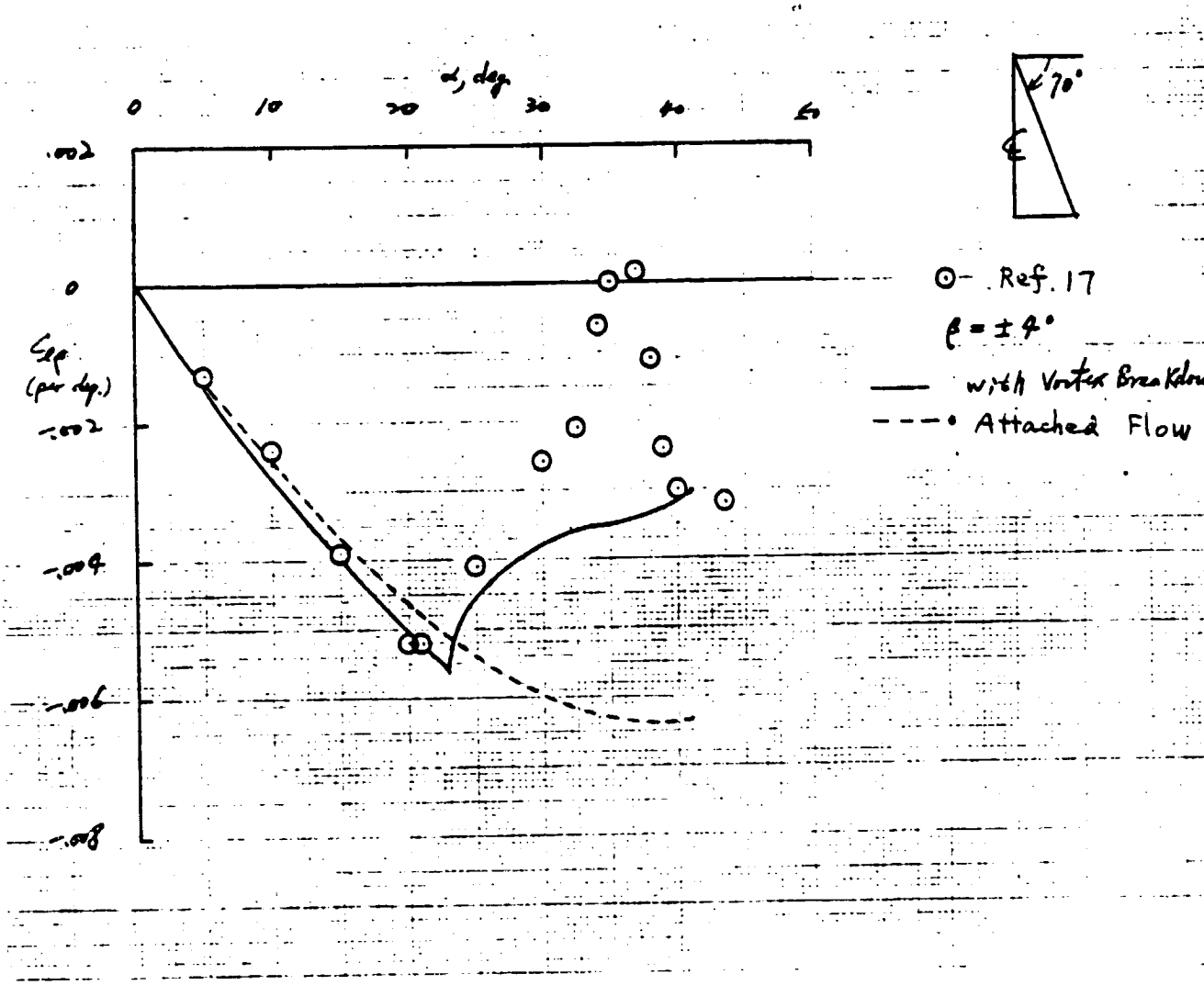

Figure 13. Delta Wing of A = 1.46 with Sharp Leading Edges

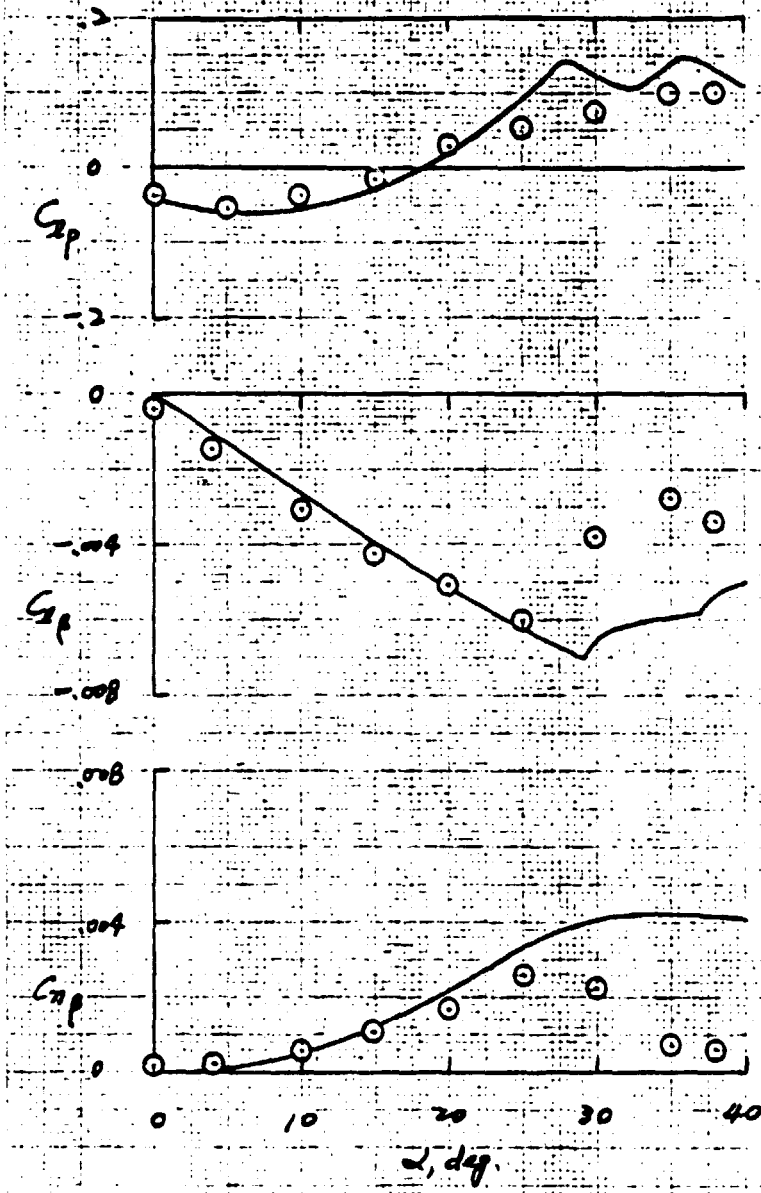

Present Theory

Data
⊙ NACA TN 1468

Figure 14 Delta Wing of $A = 1.0$ with Sharp Leading Edges and $\beta = \pm 4°$ and $\bar{p} = .1$

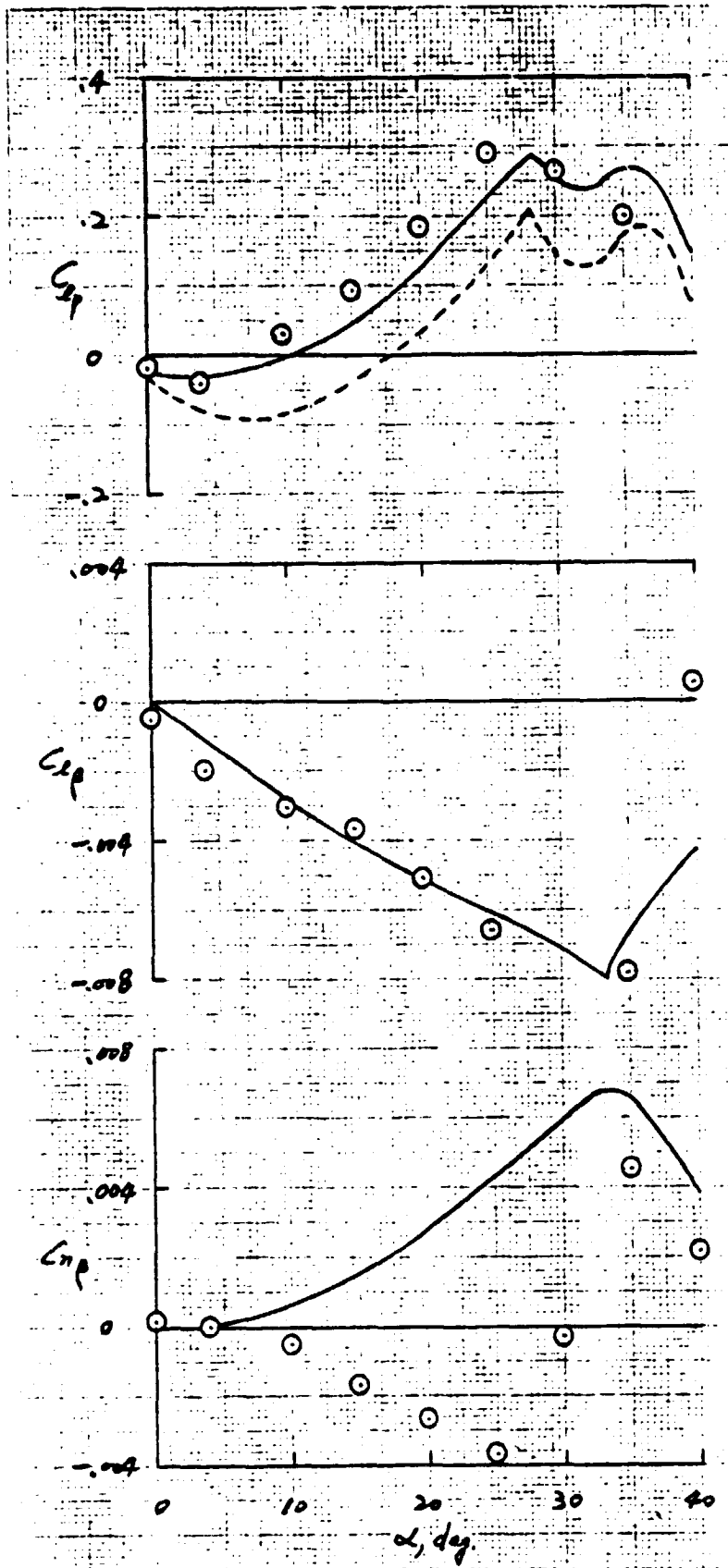

Present Theory

——— with Boundary Layer Correction

– – – – – without Boundary Layer Correction

Data

⊙ NACA 146B

Figure 15 Delta Wing of $A = 0.5$ with Sharp Leading Edges and $\beta = \pm 5°$ and $\bar{\rho} = .1$

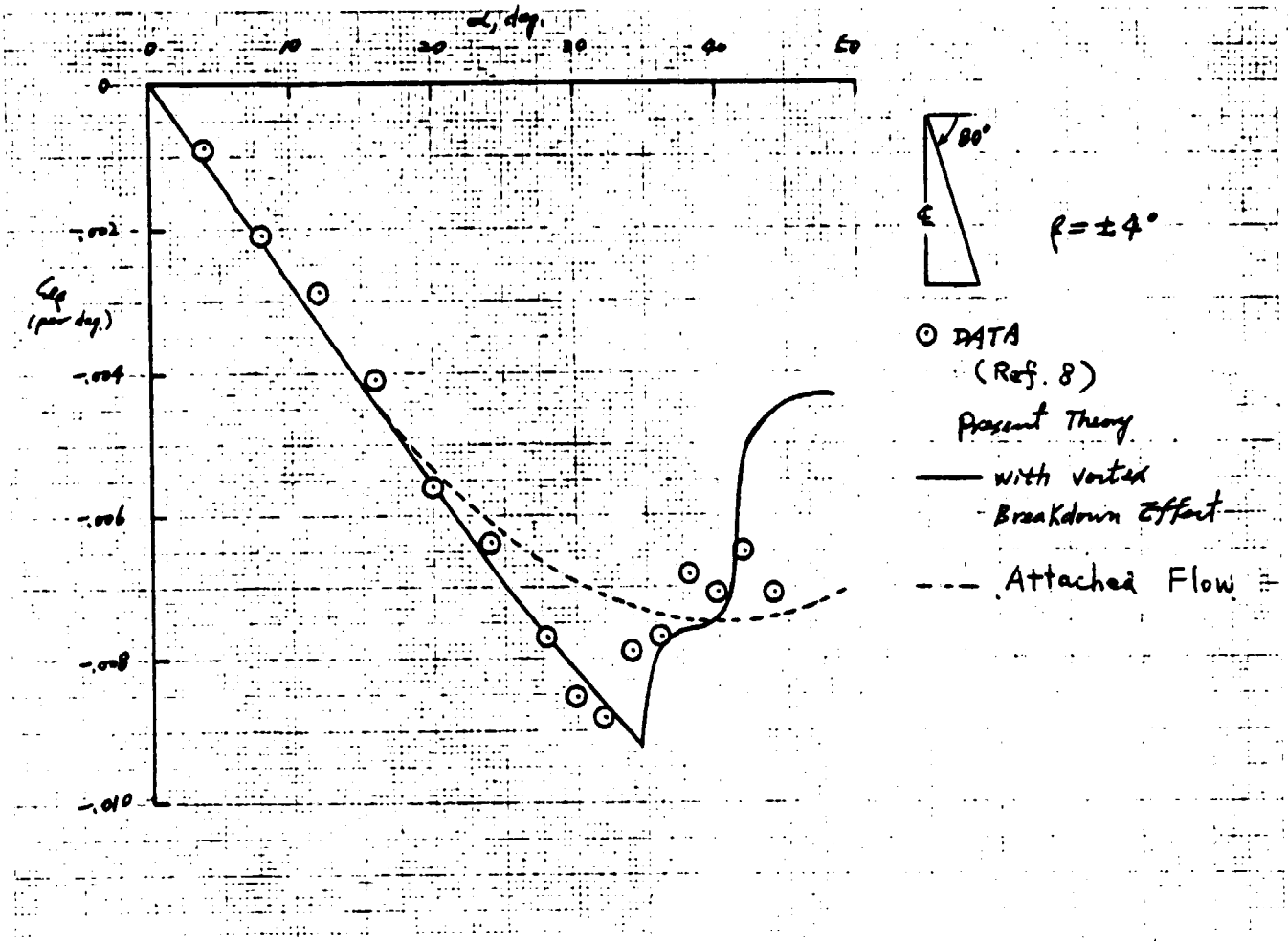

Figure 16. Lateral-stability Derivative with α for a Delta Wing of $A = 0.705$ with Sharp Leading Edges with $\beta = \pm 4°$

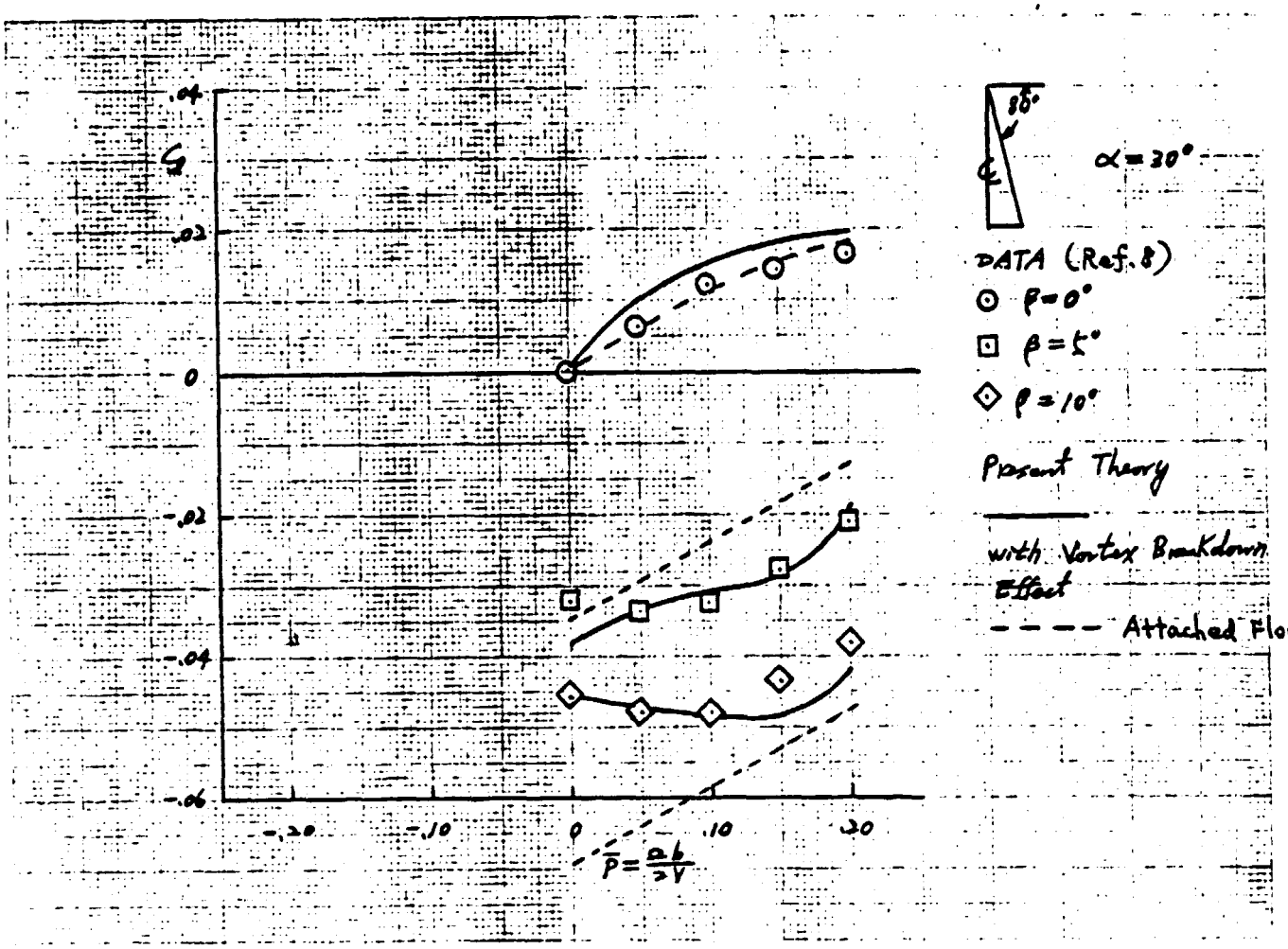

Figure 17. Effect of Sideslip on Roll Damping